Full Paper

Propellants, Explosives, Pyrotechnics

DOI: 10.1002/prep.201800309

Study on Burning and Thermal Decomposition Properties of HTPB Propellant Containing Synthesized Micro-nano Ferric Perfluorooctanoate

Fei Zhen,[a] Xu-Yuan Zhou,[a] Li-Qiong Wang,*[a] Rong-Jie Yang,[a] and Feng-Lei Huang*[a]

Abstract: A novel micro-nano ferric perfluorooctanoate [$Fe(PFO)_3$] was prepared and added in AP/Al/HTPB composite solid propellant as a catalyst to study its effects on burning and thermal decomposition properties of the propellant. To further discuss the possible thermal mechanism of the propellant containing $Fe(PFO)_3$, the major effects of $Fe(PFO)_3$ catalyst on Al were investigated by differential scanning calorimetry (DSC), thermogravimetric analysis (TG) and X-ray diffraction (XRD). Results show that By adding 3 w.t.% $Fe(PFO)_3$, the burning rate could increase by 27.8% at 3 MPa, meanwhile, the pressure exponent decreased. The aggregation/agglomeration process of the propellant containing $Fe(PFO)_3$ efficiently suppressed, and the particle size of condensed combustion products decreased clearly. In addition, $Fe(PFO)_3$ could reduce the thermal decomposition temperature of the propellant and enhance the heat release. Thermite reaction between decomposition products of $Fe(PFO)_3$ and Al was triggered at 635 °C, resulting in heat release and formation of α-Al_2O_3.

Keywords: Ferric perfluorooctanoate · Composite solid propellant · Burning properties · Aggregation · Thermal decomposition

1 Introduction

Because of the excellent performance of hydroxyl-terminated polybutadiene (HTPB) based propellant, it has been widely applied in the field of aerospace propulsion and the exploration of the universe currently. There are many important parameters to evaluate the properties of propellants such as density, specific impulse, combustion heat release, flame temperature, burning rate and so on. Among of them, combustion performance, especially burning rate is one of the irreplaceably important combustion performances for the propellant [1,2] as increasing burning rate is beneficial to improve regional targeting capability and to suppress particles agglomeration during combustion. According to the published works, there's an intrinsic relationship between burning properties and the thermal decomposition of ammonium perchlorate (AP). It has been approved that the burning rate of AP-based composite solid propellant increases as the decomposition temperature of AP decreases [3–6]. In the past decades, the application of metal oxides and metal salts as catalysts was popularized for obtaining better decomposition properties of AP and combustion efficiency of AP-based composite solid propellant. The effects of compounds with metal irons on the decomposition of AP were investigated by other groups [7,8], who concluded that these compounds could catalyze thermal reactions and oxidizing processes. And these compounds extensively applied in chemical industries could improve catalytic effects by changing the energy barrier of thermolysis and the reaction mechanisms of the main ingredients.

CuO is one of the most remarkable metal oxide catalysts. It attracts the most attention of scholars owing to its effective catalysis on the thermal decomposition of AP and the combustion of AP-based composite solid propellant [9]. Further studies on CuO nanoparticle [10–12] and CuO/carbon nanotubes (CNTs) composite [13,14] have also been carried out for years. In addition to CuO, Fe_2O_3 also has good catalytic effect on the decomposition of AP and AP-based composite solid propellant. Fe_2O_3 can be used as not only a catalyst [15–18] but also a high-energy ingredient [19] in AP-based composite solid propellant. Fe_2O_3 could reduce activation energy and reaction temperature. For AP-based aluminized composite propellants, the mixture of Fe_2O_3 as a high-energy ingredient and micro/nano aluminum could form Al/Fe_2O_3 thermites, which could contribute more energy release and further improve the burning rate of the propellants [20]. However, it is easy for micro/nano Fe_2O_3 to aggregate to result in worse dispersion and to decrease catalytic activity. Besides, Fe_2O_3 could also increase

[a] F. Zhen, X.-Y. Zhou, L.-Q. Wang, R.-J. Yang, F.-L. Huang
State Key Laboratory of Explosion Science and Technology
Beijing Institute of Technology
Zhongguancun South Street No. 5
Beijing 100081, P.R. China
*e-mail: wlq2018@sina.com
huangfl@bit.edu.cn

the viscosity of solid propellant during processing. Therefore, it is required to overcome such deficiencies.

In our previous studies [21], ferric perfluorooctanoate $Fe(PFO)_3$ was prepared as a good catalyzer for the decomposition of AP. It was proved that $Fe(PFO)_3$ could decrease the activation energy of $Fe(PFO)_3$/AP mixture and increase total heat release of AP significantly. The thermal decomposition products of $Fe(PFO)_3$ such as Fe_2O_3, FeF_2 and FeF_3 could catalyze the thermal decomposition and decrease the decomposition temperature of AP in the range of high-temperature. Based on this result, $Fe(PFO)_3$ is expected to be a promising additive which has a good effect on the burning properties of AP-based composite solid propellant. However, the influence of $Fe(PFO)_3$ on burning and thermal decomposition properties of composite solid propellant as well as the reaction mechanism between $Fe(PFO)_3$ and aluminum are still not clear. Thereby, it's necessary to study the effects of $Fe(PFO)_3$ on AP-based composite solid propellant. In this paper, AP/Al/HTPB composite solid propellant with different content of $Fe(PFO)_3$ were prepared. The effects of $Fe(PFO)_3$ on burning properties and the thermal decomposition properties of composite solid propellant were investigated. The effects of $Fe(PFO)_3$ on Al were studied further.

2 Experimental Section

2.1 Materials

Hydroxyl terminated polybutadiene (HTPB binder), diisooctyl sebacate (DOS), 2,4-toluene diisocyanate (TDI), and ammonium perchlorate (AP) required for this study were purchased from HuiAn chemical industry Co., Ltd., China. Aluminum powder was obtained from Yuanyang Aluminum Industry Co., Ltd., China. The particle size distribution of aluminum powder was 4–6 μm. $Fe(PFO)_3$ was synthesized in the laboratory by a reported procedure [21]. Two types of AP particle size (5–15 μm and 110–125 μm) were selected in the formulations for higher propellant density.

2.2 Preparation of Samples

HTPB was used as binder. DOS and TDI were used as plasticizer and the curing agent, respectively. AP/Al/HTPB composite solid propellant was formulated. Propellant sample S0 without $Fe(PFO)_3$ was prepared as basic formula. As to AP/Al/HTPB composite solid propellant containing $Fe(PFO)_3$, AP/$Fe(PFO)_3$ mixture was grindingly mixed firstly in order to disperse $Fe(PFO)_3$ into HTPB matrix much better [22]. Sample S1 and S2 with 1.5 wt.% and 3 wt.% $Fe(PFO)_3$ were prepared respectively. The slurry was cured in an incubator at 60 °C for 7 days.

To further study the effect of $Fe(PFO)_3$ on aluminum, pristine aluminum powder, pristine $Fe(PFO)_3$ and Al/$Fe(PFO)_3$ mixture samples were also prepared. The mass fraction of $Fe(PFO)_3$ in Al/$Fe(PFO)_3$ mixture was 14.3 wt.%. The mass ratio of $m_{Al}:m_{Fe(PFO)3}$ was 18:3. The formulations of samples are given in Table 1.

Table 1. Composition of prepared samples.

Samples	HTPB binder/wt.%	Al/wt.%	AP/wt.%	Fe(PFO)3/wt.%
S0	15	18	67	–
S1	15	18	65.5	1.5
S2	15	18	64	3.0
P0	–	100	–	–
P1	–	–	–	100
P2	–	85.7	–	14.3

2.3 Characterization of Burning Properties

Samples were made into cubic rod with dimensions of $5 \times 5 \times 25$ mm for the measurements. To ensure uniform ignition, a conventional nichrome wire was used to ignite the samples. The burning rates of samples under 3 MPa, 5 MPa, 7 MPa and 9 MPa were measured by the measuring system [23, 24] at room temperature. And to obtain burning rate accurately, the burning data in first 5 mm and last 5 mm were omitted. Test results in Table 2 are average of the 3 experiments under the same conditions. The burning characters on the surface of propellant in the presence or absence of $Fe(PFO)_3$ were recorded by high-speed video recording system under 0.1 MPa in the atmosphere of argon. Scanning electron microscope (SEM) was used to evaluate morphology and shape of condensed combustion products, and size distribution of condensed combustion products was measured by Laser particle size analyzer.

Table 2. Parameters *a* and *n* of Propellant Samples in Vieille's Law.

Samples	*a*	*n*
S0	3.673	0.479
S1	4.831	0.412
S2	4.928	0.420

2.4 Thermal Properties Analysis

The influence of $Fe(PFO)_3$ on decomposition of propellant samples were determined by thermal gravity (TG) and differential scanning calorimetry (DSC). TG analysis was carried out by Pyris Diamond TG instrument with a heating rate of 10 °C min^{-1} from 50 °C to 700 °C in argon atmosphere at 60 mL min^{-1}. DSC analysis was carried out by STA 449 F3 Jupiter® instrument with 10 °C min^{-1} heating rate in nitrogen

atmosphere at 50 mL min^{-1}. The Sample used in the analysis is about 2 mg.

The thermal performances of pristine Al, Fe(PFO)$_3$, and mixture of Al and Fe(PFO)$_3$ were also carried out in the same way above as a comparison. Further thermal decomposition products of Al/Fe(PFO)$_3$ was analyzed by X-ray diffractometer with Cu K_α radiation from 10° to 80°. These products were collected by tube furnace in argon flow. These products were collected by tube furnace from 50 °C to 700 °C at 10 °C min^{-1} in argon atmosphere.

3 Results and Discussion

3.1 Burning Properties of Propellant Samples

The burning rate is one of the important parameters for the propellant. The plots of burning rate vs. pressure for S0, S1 and S2 are presented in Figure 1. The values of *a* and *n* are fitted in Vieille's law and summarized in Table 2. As it can be seen, the burning rates for S1 and S2 with Fe(PFO)$_3$ distinctly went up compared with that for the original propellant formulation S0. The more addition of Fe(PFO)$_3$ was, the higher burning rate was. Compared with S0, the burning rates for S2 with 3 w.t.% Fe(PFO)$_3$ increased by 27.8%, 22.4%, 17.8% and 21.0% at 3, 5, 7 and 9 MPa respectively. Besides, the pressure exponents (0.412 and 0.420) for S1 and S2 were lower than that (0.479) for S0. High burning rate contributes to more rapid heat release and small pressure exponent would make propellant more insensitive to ambient pressure during combustion. It means that the combustion behavior of composite solid propellant containing Fe(PFO)$_3$ was more stable than that of original propellant under the condition of dynamic pressure.

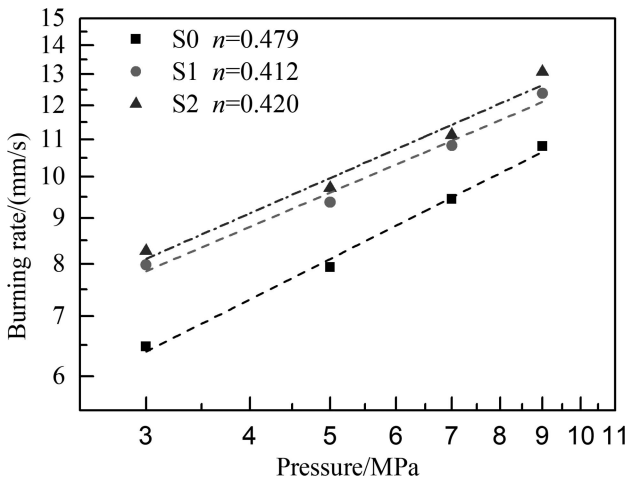

Figure 1. Burning rates of AP/Al/HTPB solid propellants with different content of Fe(PFO)$_3$.

To further characterize the combustion process of propellant samples, the burning characters on the surface of samples were recorded by a high-speed video recorder under 0.1 MPa in the atmosphere of argon. The sequential screenshots from the video are presented in Figure 2. Qualitative information about the aggregation/agglomeration process and the morphology of burning surface could be observed. As shown in Figure 2 (a), the ignited aluminum particles in the sample S0 agglomerated heavily on the conical burning surface during the combustion. Agglomerate was large and irregular and its size was about 100 μm. As a contrast, the ignited aluminum particles were found splashing from the planar burning surface of solid propellant S2 in Figure 2 (b). These burning particles were smaller and more regular than that of S0.

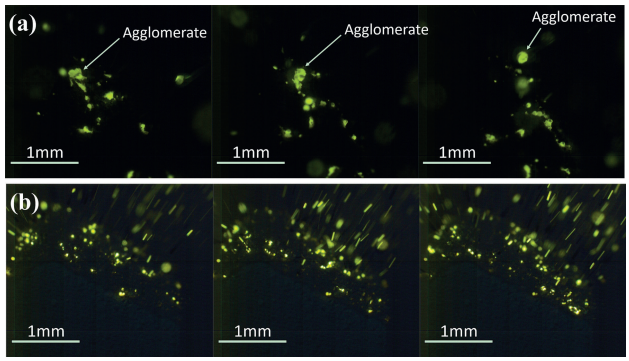

Figure 2. Screenshots of combustion process for S0 (a) and S2 (b) at 0.1 MPa in argon under 4500 fps.

To obtain the static particle size distribution of condensed combustion products, SEM was used to evaluate the morphology and shape of the condensed combustion products of propellants S0 and S2. Comparisons of SEM images for propellants S0 and S2 are shown in Figure 3. For propellant S0, there were many large particles in the condensed combustion products, and the surface of the large particles was covered with plenty of small particles combustion products. What's more, small particles were converged

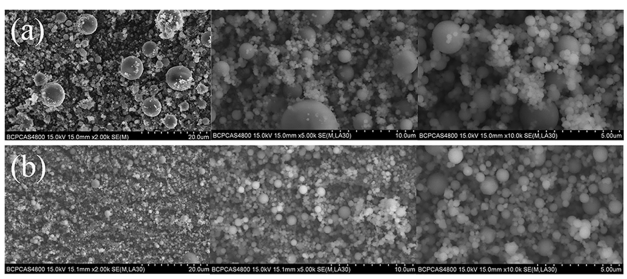

Figure 3. SEM images of condensed combustion products of S0 (a) and S2 (b). The magnification of the micrograph from left to right is 2000, 5000 and 10000 times respectively.

and formed many large agglomerates. Compared with S0, there were no obvious large combustion products in condensed combustion products of S2. Therefore, adding Fe(PFO)$_3$ to AP/Al/HTPB composite solid propellant, large particles in the combustion products were reduced, and the agglomeration was weakened.

Figure 4 presents the collected condensed combustion products size distribution of propellants S0 and S2. The size of the combustion products of S0 was mainly distributed in four ranges, 0.1–0.3 μm, 0.3–1.0 μm, 1.0–13.2 μm and 13.2–182.0 μm successively. Comparison of particle size distribution of condensed combustion products of S0 and S2, the maximum particle size of S2 (45.709 μm) condensed combustion products was obviously lower than that of S0 (181.970 μm). The volume fraction of S2 in the range of 1.0–13.2 μm increased significantly, and decreased in the range of 13.2–182.0 μm. The results show that coarse condensed combustion products particles decreased and fine particles (below 13.2 μm) increased with the addition of Fe(PFO)$_3$. In addition, the condensed combustion products size distribution of S0 and S2 both show four distinct peak values in Table 3. Compared with S0, the D_{10} and D_{50} of S2 condensed combustion products did not change significantly, while D_{90} and D_v decreased 64.2% and 54.1% respectively. And the R of S2 was reduced by 66.9%. In short, the results show that adding Fe(PFO)$_3$ in composite solid propellant could reduce the particle size of condensed combustion products as well as narrow the size distribution of condensed combustion products.

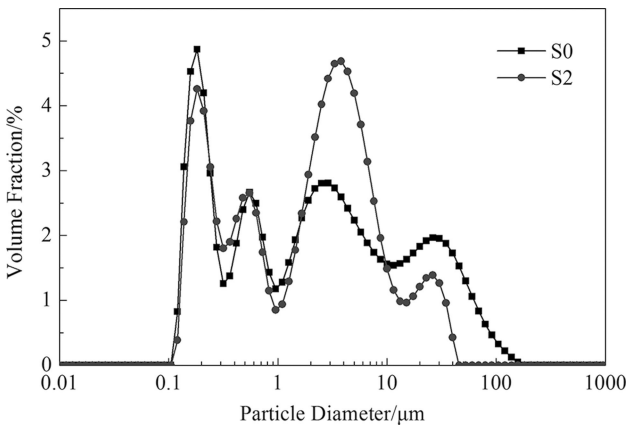

Figure 4. Condensed combustion products size distribution of propellants S0 and S2.

Table 3. Particle sizes data in propellants S0 and S2.

Samples	D_{10}[(a)]/μm	D_{50}[(b)]/μm	D_{90}[(c)]/μm	D_v[(d)]/μm	R[(e)]
S0	0.190	2.360	35.040	10.865	14.760
S2	0.205	2.520	12.541	4.985	4.895

[(a–c)] D_{10}, D_{50} and D_{90} represent the particle size corresponding to the cumulative size distribution percentage of 10%, 50% and 90% respectively. [(d)] D_v represents volume average particle size. [(e)] $R=(D_{90}-D_{10})/D_{50}$, means the uniformity of particle size distribution.

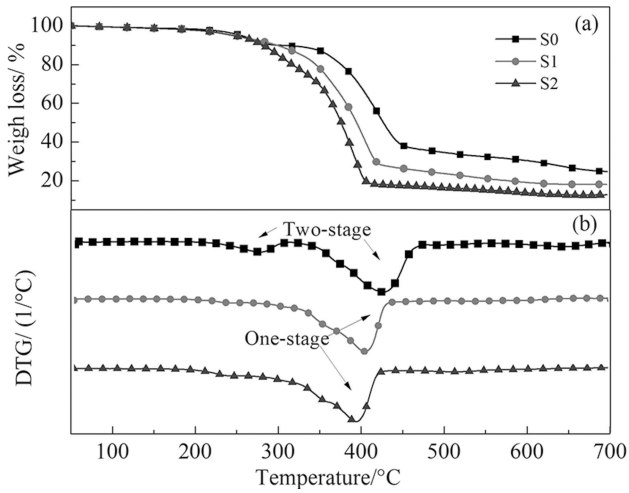

Figure 5. TG (a), DTG (b) curves of the solid propellant samples.

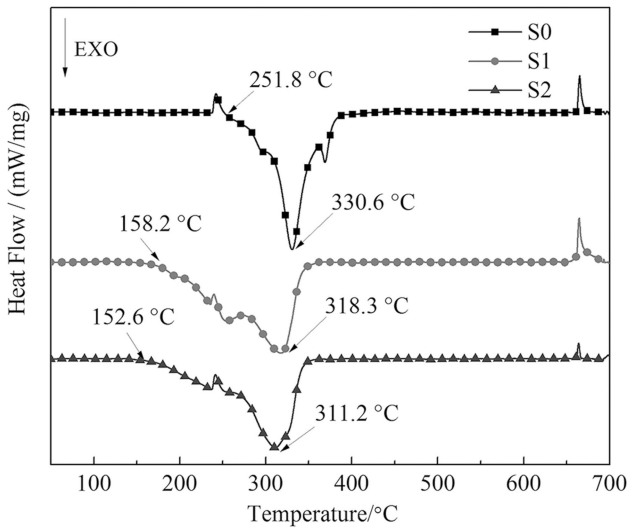

Figure 6. DSC curves of the solid propellant samples.

3.2 Thermal Properties of Samples

The analysis results by TG (DTG) and DSC are shown in Figure 5 and Figure 6 respectively. TG curves indicate that for AP/Al/HTPB composite solid propellant (S0) there was a three-stage weight loss in the temperature range of 50–700 °C. The weight loss for first two stages from 260 °C to 430 °C was owing to the decomposition of pristine AP. The weight loss for the third stage from 430 °C to 700 °C was considered to be from the continuous pyrolysis of polymer binder. However, for samples (S1 and S2) containing Fe(PFO)$_3$ catalyst, there were a two-stage decomposition. In the

case of S1, the first stage from 260 °C to 410 °C corresponds to the decomposition of AP about 70 % weight loss, and the second stage from 410 °C to 700 °C corresponds to the complete decomposition of propellant samples into gaseous products about 10 % weight loss. And with the increase of $Fe(PFO)_3$, weight loss increased as well as thermal decomposition temperature declined. According to our previous study [21], $Fe(PFO)_3$ could decrease the decomposition temperature of AP in the range of high-temperature, which was considered as the main reason for the two-stage weight loss merging into one-stage weight loss from 430 °C to 410 °C in Figure 5 (b).

Further DSC analysis for the thermal decomposition of propellant samples were also investigated as shown in Figure 6. Such endothermic/exothermic peaks of S0 could be easily distinguished as: the endothermic peak from 240 °C to 250 °C was attributed to the phase transformation of AP; a series of consecutive exothermic peaks from 250 °C to 400 °C were respected to the contribution of decomposition of AP with two types of particle size and partial oxidization of aluminum; the endothermic peak at 660 °C belonged to the melting point of residual aluminum. DSC thermogram of S0 reveals that the thermic process of the propellant sample tends to be a superposition of each component under a low heating rate 10 °C min^{-1}.

As involved in Figure 6, samples containing $Fe(PFO)_3$ presented more particular exothermic peaks for the decomposition of the propellants. First of all, the position of their exothermic peaks was ahead of S0. The onset exothermic peak appeared before the phase transition of AP. The onset exothermic temperatures for samples S1 and S2 were 158.2 °C and 152.6 °C lower than that for samples S0. And the exothermic peak temperatures were respectively about 12.3 °C and 19.4 °C lower than that of S0. These results were in accordance with that by TG (DTG) analysis. It means that the presence of $Fe(PFO)_3$ made the decomposition of AP easier.

Moreover, the thermal decomposition data during the decomposition from 180 °C to 400 °C at 10 °C min^{-1} are listed in Table 4. The heat release for the propellant with addition of $Fe(PFO)_3$ was higher than that for propellant S0. Therefore, the micro-nano $Fe(PFO)_3$ could notably improve the initial thermal decomposition of AP/Al/HTPB composite solid propellant and enhance the heat release during the decomposition stage.

Table 4. Thermal decomposition data of samples S0, S1 and S2.

Samples	Onset temperature/°C	Peak temperature/°C	$\Delta H/kJ \cdot g^{-1}$
S0	251.8	330.6	1.72
S1	158.2	318.3	2.01
S2	152.6	311.2	2.24

3.3 The Interactions between $Fe(PFO)_3$ and Al

To further study the mechanism of $Fe(PFO)_3$ on AP/Al/HTPB composite solid propellant, it is necessary to investigate the interactions between Al and $Fe(PFO)_3$. DSC curves for the mixture are demonstrated in Figure 7, and TG-DSC curves of the pristine $Fe(PFO)_3$ are presented in Figure 8. Upon heating, the pristine Al underwent the phase transition at 660 °C (melting point). As for Al/$Fe(PFO)_3$ mixture, an obvious exothermic peak before the melting point of aluminum about 635 °C was observed. There was a severe heat release with fast chemical reaction at 635 °C. DSC curve in Figure 8 shows that two distinct exothermic peaks during thermal decomposition of $Fe(PFO)_3$ were just located on 267 °C and 340 °C respectively lower than 635 °C. Thus, the exothermic peak in Figure 7 could be the reaction between aluminum and decomposition products of $Fe(PFO)_3$.

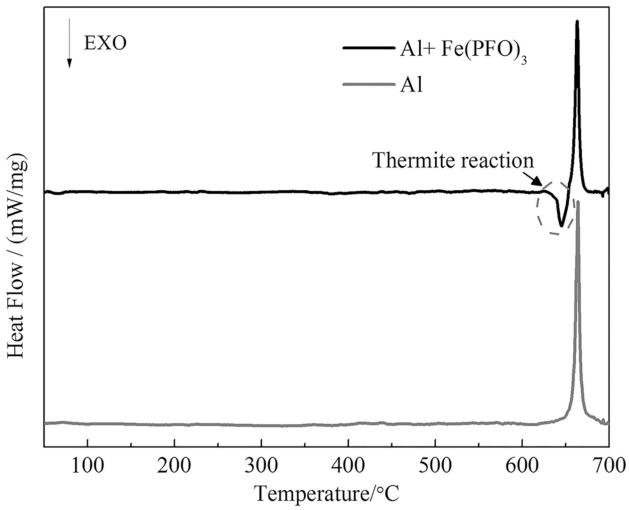

Figure 7. DSC curves of Al/$Fe(PFO)_3$ mixture and pristine Al.

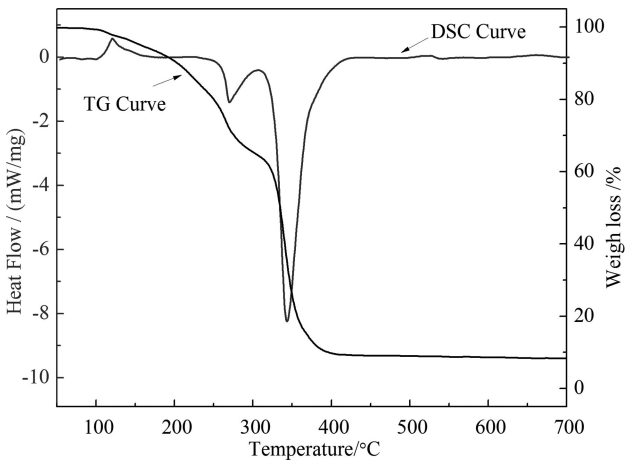

Figure 8. DSC and TG curves of pristine $Fe(PFO)_3$.

Based on above analysis, the mixture of Al and $Fe(PFO)_3$ was heated by tube furnace below 700 °C with argon flow. Then, the heat-treated products were collected and characterized by XRD analysis to get insights into its reaction mechanism. Figure 9 demonstrates XRD pattern of the heat-treated products.

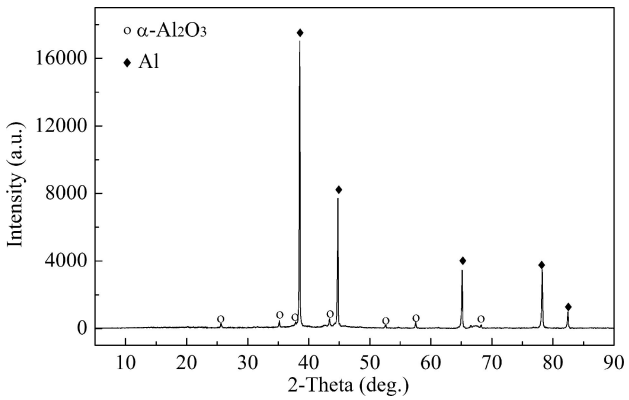

Figure 9. XRD pattern of Al/$Fe(PFO)_3$ heat-treated products under argon atmosphere.

It is very impressive that there was α-Al_2O_3 in the products after the thermal treatment according to XRD analysis. Because formation of α-Al_2O_3 needs high temperature approximately 1180 °C [25, 26], there was no enough energy provided to such crystalline transition at 700 °C. Therefore, it is supposed that the formation of α-Al_2O_3 was caused by partial fast heat release from some exothermic reaction. The decomposition products of $Fe(PFO)_3$ were Fe_2O_3, FeF_2, and FeF_3 [21]. It is postulated that the reactions between decomposition products of $Fe(PFO)_3$ and aluminum should be actually thermite reactions (between Fe_2O_3 and Al) or similar to the thermite reaction (between FeF_2, FeF_3 and Al) at 635 °C, during which there was large quantity of energy release and quick temperature rise. The high temperature led by the heat release might be a reasonable mechanism for the formation of α-Al_2O_3. Such thermite reactions were beneficial to promote the heat release of propellants and to enhance the ignition properties of aluminum powders as well.

4 Conclusions

A new ferric perfluorooctanoate $Fe(PFO)_3$ used in AP/Al/HTPB composite solid propellant was studied. It is proved that the addition of mirco-nano $Fe(PFO)_3$ could enhance the burning rate and be in favor of steady combustion of AP/Al/HTPB composite solid propellant. Micro-nano $Fe(PFO)_3$ could suppress agglomeration of aluminum particles during the combustion process for composite solid propellant. And it also could decrease the size of condensed combustion particles significantly. Moreover, based on the thermal analysis, $Fe(PFO)_3$ was considered to be a great catalyst that could decrease the thermal decomposition temperature of AP/Al/HTPB composite solid propellant, and enhance the heat release during the decomposition stage. The decomposition products of $Fe(PFO)_3$ could undergo a thermite reaction with aluminum at 635 °C resulting in large heat release and formulation of α-Al_2O_3.

References

[1] L. Liu, J. Li, L. Zhang, S. Tian, Effects of Magnesium-based Hydrogen Storage Materials on the Thermal Decomposition, Burning rate, and Explosive Heat of Ammonium Perchlorate-based Composite Solid Propellant, *J. Hazard. Mater.* **2018**, *342*, 477–481.

[2] R. Tong, Y. Zhao, L. Wang, H. Yu, F. Ren, M. Saleem, W. A. Amer, Recent Research Progress in the Synthesis and Properties of Burning Rate Catalysts Based on Ferrocene-containing Polymers and Derivatives, *J. Organomet. Chem.* **2014**, *755*, 16–32.

[3] M. Kohga, Burning Characteristics of AP/HTPB Composite Propellants Prepared with Fine Porous or Fine Hollow Ammonium Perchlorate, *Propell. Explos. Pyrot.* **2010**, *31*, 50–55.

[4] V. V. Boldyrev, Thermal Decomposition of Ammonium Perchlorate, *Thermochim. Acta* **2006**, *443*, 1–36.

[5] J. A. F. F. Rocco, J. E. S. Lima, A. G. Frutuoso, K. Iha, M. Ionashiro, J. R. Matos, M. E. V. Suárez-Iha, Thermal Degradation of a Composite Solid Propellant Examined by DSC, *J. Therm. Anal. Calorim.* **2004**, *75*, 551–557.

[6] S. Vyazovkin, C. A. Wight, Kinetics of Thermal Decomposition of Cubic Ammonium Perchlorate, *Chem. Mater.* **1999**, *11*, 3386–3393.

[7] R. Yang, H. An, H. Tan, Combustion and Thermal Decomposition of HNIW and HTPB/HNIW Propellants with Additives, *Combust. Flame* **2003**, *135*, 463–473.

[8] G. B. Manelis, G. M. Nazin, I. R. Yu, V. A. Strunin, Thermal Decomposition and combustion of Explosives and Propellants, *Crc Press* **2003**, *6*.

[9] L. Chen, L. Li, G. Li, Synthesis of CuO Nanorods and Their Catalytic Activity in the Thermal Decomposition of Ammonium Perchlorate, *J. Alloy. Compod.* **2008**, *464*, 532–536.

[10] A. A. Vargeese, K. Muralidharan, Kinetics and Mechanism of Hydrothermally Prepared Copper Oxide Nanorod Catalyzed Decomposition of Ammonium Nitrate, *Appl. Catal. A-Gen.* **2012**, *447–448*, 171–177.

[11] L. J. Chen, G. S. Li, L. P. Li, CuO Nanocrystals in Thermal Decomposition of Ammonium Perchlorate, *J. Therm. Anal. Calorim.* **2008**, *91*, 581–587.

[12] Y. Xu, D. Chen, X. Jiao, K. Xue, CuO Microflowers Composed of Nanosheets: Synthesis, Characterization, and Formation Mechanism, *Mater. Res. Bull.* **2007**, *42*, 1723–1731.

[13] Y. P. Zhang, Y. C. Jiao, Y. S. Yang, C. L. Li, Ligand-free Catalytic System for the Synthesis of Diarylethers Over Cu_2O/Cu-CNTs as Heterogeneous Reusable Catalyst, *Tetrahedron Lett.* **2013**, 6494–6497.

[14] S. Iijima, Helical Microtubules of Graphitic Carbon, *Nature.* **1991**, *354*, 56–58.

[15] L. Song, S. Zhang, B. Chen, J. Ge, X. Jia, A Hydrothermal Method for Preparation of α-Fe_2O_3 Nanotubes and Their Catalytic Performance for Thermal Decomposition of Ammonium Perchlorate, *Colloid. Surface. A.* **2010**, *360*, 1–5.

[16] H. Xu, X. Wang, L. Zhang, Selective Preparation of Nanorods and Micro-octahedrons of Fe_2O_3 and Their Catalytic Performances for Thermal Decomposition of Ammonium Perchlorate, *Powder Technol.* **2008**, *185*, 176–180.
[17] N. N. Zhao, N., C.C. He, J.G. Liu, H. J. Gong, T. An, H. X. Xu, F. Q. Zhao, R. Z. Hu, H. X. Ma, J. Z. Zhang, Dependence of Catalytic Properties of Al/Fe_2O_3 Thermites on Morphology of Fe_2O_3 Particles in Combustion Reactions, *J. Solid. State. Chem.* **2014**, *219*, 67–73.
[18] S. S. Joshi, P. R. Patil, V. N. Krishnamurthy, Thermal Decomposition of Ammonium Perchlorate in the Presence of Nanosized Ferric Oxide, *Defence. Sci. J.* **2008**, *58*, 721–727.
[19] P. Liu, J. R. Kong, X. D. Xu, F. L. Sun, Q. C. Liu, Preparation and Catalytic Activity of Fe_2O_3/CNT to Thermal Decomposition of Ammonium Perchlorate, *Adv. Mater. Res.* **2012**, *396–398*, 837–840.
[20] Q. L. Yan, F. Q. Zhao, K. K. Kuo, X. H. Zhang, S. Zeman, L. T. Deluca, Catalytic Effects of Nano Additives on Decomposition and Combustion of RDX-, HMX-, and AP-based Energetic Compositions, *Prog. Energ. Combust.* **2016**, *57*, 75–136.
[21] P. Tu, M. Zou, R. Yang, X. Guo, Synthesis of Ferric Perfluorooctanoate [$Fe(PFO)_3$] and its Catalysis on Thermal Decomposition of Ammonium Perchlorate, *Thermochim. Acta* **2016**, *646*, 32–38.
[22] J. Xu, Z. Y. Ma, M. X. Zha, F. Q. Zhao, Preparation and Characterization of CuO/AP/HTPB Energetic Nanocomposites, *Acta Armamentarii* **2013**, *34*, 547–553.
[23] Z. Liu, S. Li, M. Liu, D. Guan, X. Sui, N. Wang, Experimental Investigation of the Combustion Products in an Aluminized Solid Propellant, *Acta Astronaut.* **2017**, *133*, 136–144.
[24] R. Yang, Y. Li, Y. Liu, Z. Hua, Advanced System of Monitor and Measurement for the Combustion Process and Rate of Solid Propellants, *J. Propul. Techno.* **2000**, *21*, 86–88.
[25] G. Bolelli, V. Cannillo, R. Gadow, A. Killinger, L. Lusvarghi, T. Manfredini, P. Müller, Properties of Al_2O_3 Coatings by High Velocity Suspension Flame Spraying (HVSFS): Effects of Injection Systems and Torch design, *Surf. Coat. Tech.* **2015**, *270*, 175–189.
[26] R. J. Damani, D. Rubeša, R. Danzer, Fracture Toughness, Strength and Thermal Shock Behaviour of Bulk Plasma Sprayed Alumina – Effects of Heat Treatment, *J. Eur. Ceram. Soc.* **2000**, *20*, 1439–1452.

Manuscript received: October 10, 2018
Version of record online: January 11, 2019

